A Low-Scattering Tightly Coupled Dipole Array in a Triangular Lattice

Liang JU [1,2], Jia-Jia REN [1], Zong-Qiang ZHANG [2], Chun-Liang DAI [2], Yu MAO [1,2], Ke HUO [1], Kun WEI [1], Wei HU [1], Wen JIANG [1]*

[1] National Key Laboratory of Radar Detection and Sensing, Xidian University, Xi'an 710071, Shaanxi, China
[2] National Key Laboratory of Electromagnetic Information Control and Effects, Shenyang Aircraft Design and Research Institute, Shenyang, China

juliang1457@qq.com, 2563604910@qq.com, zhangzq0601@163.com, cldaixmu@163.com, maoyu0807@163.com, huo_ke@qq.com, weikun@xidian.edu.cn, weihu.xidian@ieee.org, jiangwen13@vip.qq.com

Submitted October 14, 2025 / Accepted July 7, 2026 / Online first September 22, 2026

Abstract. *A low-scattering tightly coupled phased array antenna based on a triangular lattice with resistive metallic strips is presented in this paper. Resistive metallic strips are loaded orthogonal to the dipole at the wide-angle impedance matching (WAIM) layer to achieve an in-band low-scattering array design. Compared to a rectangular grid, a triangular grid phased array reduces the total number of elements by approximately 13.4%. The proposed array achieves ±45° beam scanning in the E- and H-planes over the frequency band of 5.6–16 GHz, while exhibiting outstanding low-scattering characteristics for cross-polarized waves throughout the operational bandwidth. The monostatic RCS reduction exceeds 10 dB within the range of 6.6–16 GHz, and it also demonstrates excellent bistatic RCS reduction under oblique incidences. A 10×10 array prototype is fabricated and measured. Both simulated and measured results are in good agreement, validating the feasibility of the design.*

Keywords

Antenna array, triangular lattice, radar cross section (RCS)

1. Introduction

With the continuous development of electromagnetic stealth technology, the electromagnetic scattering levels of stealth combat platforms have been significantly reduced through shape design and the application of absorptive materials. The phased array antenna mounted on the platform emerges has emerged as the primary scattering source under the backdrop. Compared with conventional phased arrays, tightly coupled phased arrays exhibit superior broadband and wide-angle scanning characteristics due to the strong coupling between elements, offering significant advantages in practical applications [1–3]. However, the inherently dense element configuration of the tightly coupled array presents considerable challenges for achieving effective low-scattering designs. In recent years, various works for RCS reduction of tightly coupled dipole arrays have been proposed, such as low-scattering arrays based on polarization-selective metamaterial absorbers [4], phased arrays employing phase-cancellation mechanisms [5], scattering control of conformal tightly coupled arrays [6], [7], and low-scattering phased arrays incorporating multifunctional metasurface [5]. Despite positive progress in these works, achieving efficient and universal RCS reduction while maintaining broadband and wide-angle scanning performance remains a significant challenge.

By employing a triangular lattice configuration, the number of elements can be reduced without changing the aperture size, thereby lowering the overall cost of phased array antennas [8]. The configuration has been widely employed in various types of array antenna designs, such as planar printed ultrawideband phased arrays [9], [10], microstrip phased arrays with substrate integrated cavities [11], Vivaldi arrays [12], and metallic arrays [13], [14]. However, research on low-scattering designs for phased arrays with a triangular lattice remains relatively limited. In [15], a Vivaldi array with a triangular grid is proposed. By introducing slits along the profile of nonradiating edges in each unit, the structural modal and antenna modal scattering currents can be separated, which achieves wide-angle in-band scattering suppression and maintains radiation performance. Although relevant studies have demonstrated the feasibility of triangular grid arrays in low-scattering designs, the applicability remains constrained to specific structures and frequency bands. Therefore, achieving efficient and broadband scattering suppression while maintaining the radiation performance of a triangular grid array remains an area that requires further investigation.

In this work, a low-scattering coupled phased array antenna based on a triangular lattice with resistive metallic strips is presented. The design is proposed by loading resistive metallic strips at the WAIM layer to achieve the in-band low-scattering property. A 10×10 array prototype is

DOI: 10.13164/re.2026.0455

fabricated and measured to validate the proposed array, with a significant monostatic RCS reduction. Meanwhile, the proposed array presents the band of 5.6–16 GHz with ±45° scanning in the E-/H-planes.

2. Low Scattering Tightly Coupled Antenna Design

2.1 Triangular Lattice Phased Array Antenna Principle

Figure 1 shows a triangular grid array with large spacing [16]. The elements are arranged in the xoy plane with spacing d_x and d_y, and the base angle of the triangle is γ. This array can be regarded as the superposition of two rectangular arrays with element spacing $2d_x \times d_y$. The condition for eliminating lobe formation in this array is:

$$d_x \le \frac{\lambda}{1+\left|\sin\theta_{0x}\right|}, \quad d_y \le \frac{1}{\sin\gamma}\frac{\lambda}{1+\left|\sin\theta_{0y}\right|}. \qquad (1)$$

For square and equilateral triangular arrays, when two phased array antennas achieve identical angle scanning in both dimensions, with $d_x = d_y = d_0$ and $\gamma = 60°$, it can obtain $\theta_{0x} = \theta_{0y} = \theta_0$. The area occupied by each array element corresponds to the blue shaded region in Fig. 1, which can be represented as

$$A_{\text{square-grid}} = d^2, \quad A_{\text{triangular-grid}} = \frac{2d^2}{\sqrt{3}}. \qquad (2)$$

Equation (2) indicates that for arrays of identical aperture dimensions, the equilateral triangular array configuration requires 13.4% fewer elements than a square grid. This reduction in the number of T/R modules yields significant cost savings. Therefore, the triangular lattice is adopted for the reference antenna array and the proposed low-scattering array.

2.2 Design of Basic Antenna Units

The designed broadband tightly coupled antenna is shown in Fig. 2. It serves as the reference antenna for performance comparison. The antenna consists of four dielectric layers with a relative permittivity of $\varepsilon_r = 2.2$ and a profile height of 0.294 λ_h. The first layer provides structural support. The dipole arms are printed on the upper surface of Layer2, with coupled patch C_1 and patch C_2 enhancing electromagnetic coupling between antenna units. Coupled patch C_1 is printed on the upper surface of Layer2, while coupled patch C_2 is printed on the upper surface of Layer1. Both layers are connected to the metal ground plane via metal shorting columns. The WAIM layers consist of a dielectric substrate Layer3 and a metasurface overlay Layer4 [17], which together cover the dipole to enhance the antenna's broadband and wide-angle scanning performance, as shown in Fig. 2(b). Moreover, Layer1 to Layer3 incorporate dielectric vias to reduce the effective dielectric constant and suppress surface wave effects. The antenna is excited via unbalanced feeding, with the inner conductor of the feed line connected to one end of the dipole arm and the outer conductor bonded to the metal ground plane. However, unbalanced feeding leads to common-mode resonance, which is shifted out of the operating frequency band by means of shorting pillars. Furthermore, the reference antenna has a maximum operating frequency of 16 GHz. Considering the condition for eliminating lobe formation under an equilateral triangular grid arrangement as specified in (1), the final unit dimensions are determined to be 9.2 mm × 10.6 mm, equivalent to $0.49 \times 0.57\ \lambda_h^2$. The main parameters of the reference antenna are shown in Tab. 1.

Figure 3 shows the boundary condition settings and triangular lattice array simulation model of the reference antenna in HFSS. Three pairs of periodic boundary conditions are used to realize the triangular lattice array, and Floquet port excitation is used to simulate the infinite array.

Figure 4 presents the active VSWR for the E-plane and H-plane at different scanning angles of the reference antenna. Simulation results show that this antenna unit exhibits excellent broadband performance in 5.6–16 GHz band for ±45° scanning in both the E-plane and H-plane.

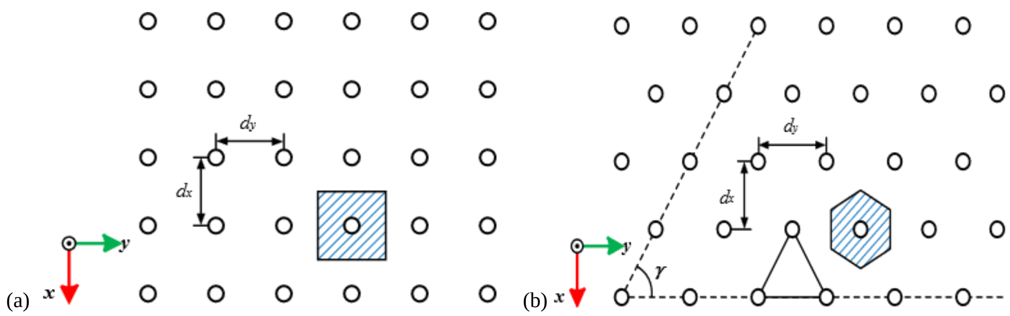

Fig. 1. Schematic diagram: (a) rectangular lattice and (b) triangular lattice.

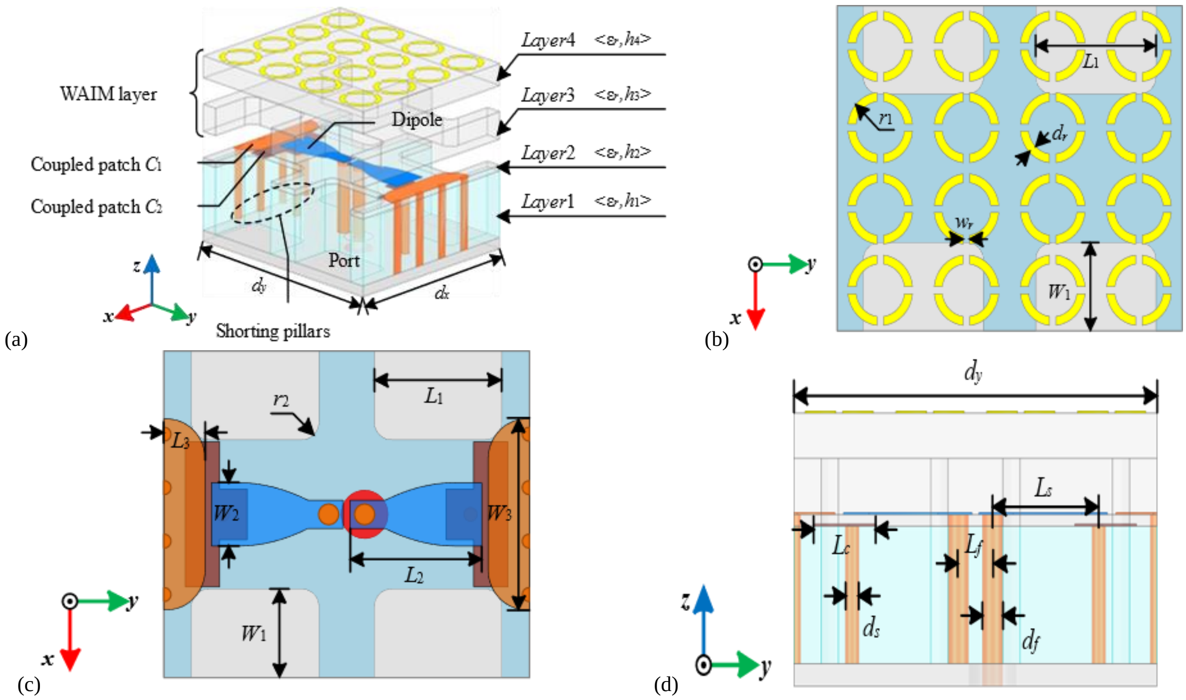

Fig. 2. Structure of the reference tightly coupled antenna: (a) 3-D view; (b) WAIM layer; (c) Dipole layer; (d) Side view.

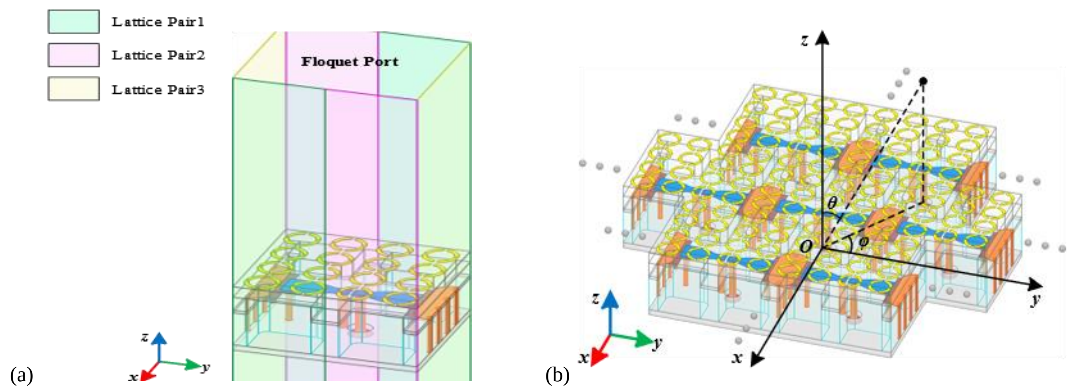

Fig. 3. Simulation model: (a) Triangular grid array under periodic boundary conditions and (b) infinite array model.

Parameters	d_x	d_y	h_1	h_2	h_3	h_4	r_1
Value/mm	9.2	10.6	3.0	0.254	1.25	1.0	1.0
Parameters	d_r	w_r	r_2	L_1	W_1	L_2	W_2
Value/mm	0.25	0.2	0.5	3.7	2.5	3.75	1.8
Parameters	L_3	W_3	d_f	d_s	L_f	L_s	L_c
Value/mm	1.2	5.2	0.6	0.4	3.6	3.1	1.8

Tab. 1. Design parameters of the proposed antenna.

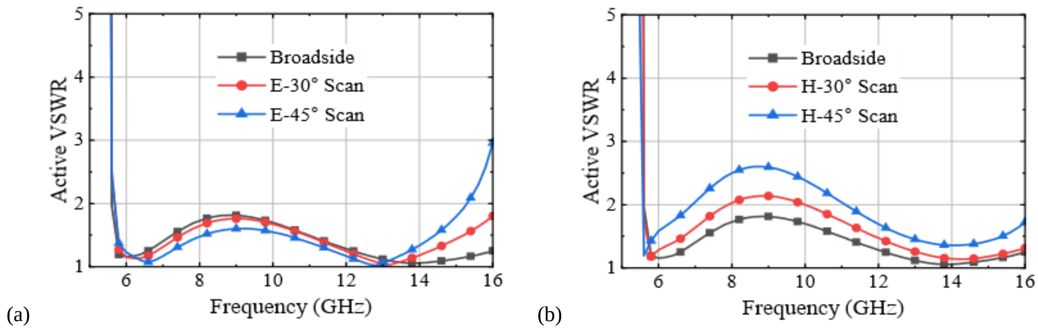

Fig. 4. Simulated VSWRs of the reference tightly coupled antenna under periodic boundary conditions: (a) E-plane; (b) H-plane.

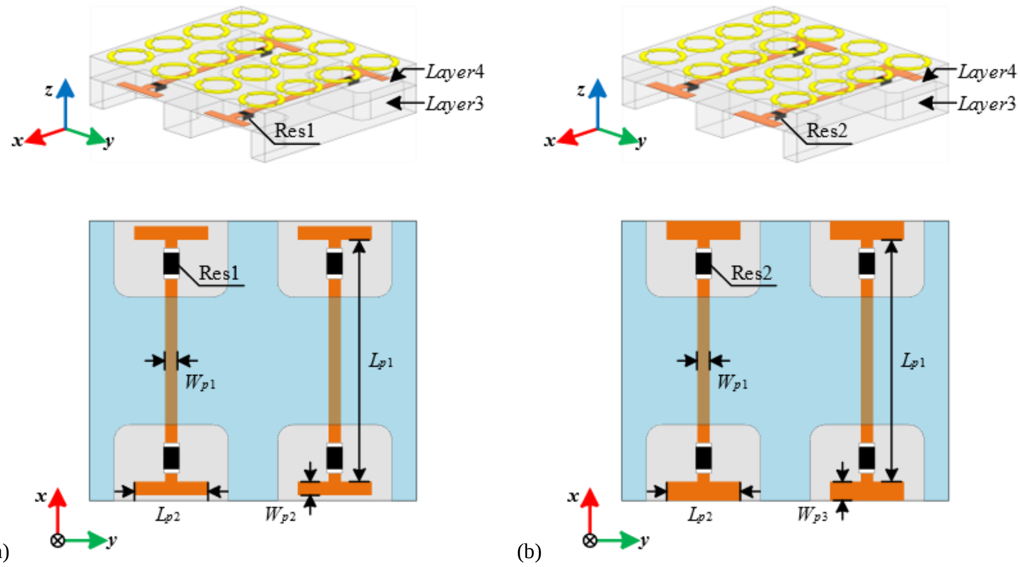

Fig. 5. Local structural model of a low-scattering antenna with different resistors and parameters: (a) Unit-A with Res1; (b) Unit-B with Res2.

2.3 Design of Basic Antenna Units

To achieve low-scattering characteristics of the cross-polarized wave, resistive strips are integrated at the base of the overlying Layer4. The local structural model is shown in Fig. 5(a), with this low-scattering antenna designated as Unit-A. Each antenna unit comprises two metal strips orthogonal to the dipole, each strip loaded with a resistor of value Res1. The parameters are as follows: L_{p1} = 7.95 mm, W_{p1} = 0.4 mm, L_{p2} = 2.4 mm, W_{p2} = 0.45 mm, Res1 = 160 Ω.

Figure 6 shows the variation curves of the reflection coefficient and absorption rate of Unit-A with frequency under vertically incident cross-polarized waves. It can be observed that reflection coefficient remains below −10 dB within 5.6–16 GHz band, while the absorption rate exceeds 80% range from 5 to 16 GHz. However, the unit exhibits a relatively high reflection coefficient within the 9–12 GHz band. To enhance RCS reduction performance in the frequency band, a low-scattering antenna Unit-B is proposed, as illustrated in Fig. 5(b).

Figure 7 shows the variation of the reflection coefficient with frequency for Unit-B when loaded with resistors of different values under cross-polarized wave incidence. It can be seen that as the resistance of Res2 increases from 200 Ω to 300 Ω, the resonant frequency shifts significantly to lower frequencies. This phenomenon is attributed to the fact that the resistance not only dissipates electromagnetic energy but also alters the effective circuit parameters of the unit, thereby changing the imaginary part of the input impedance and causing a shift in the resonant point. Considering the antenna's frequency band and the requirement to maintain a reflection coefficient below −10 dB, Res2 is set to 250 Ω. With this configuration, the resistance not only effectively dissipates energy but also optimizes the input impedance of Unit-B, enabling good absorption performance over a wide bandwidth. As expected, Unit-B maintains reflection coefficients below −15 dB across the 10–14.6 GHz range, demonstrating excellent low-scattering characteristics for cross-polarized waves. In this setting, Unit-B is designed with W_{p3} = 0.625 mm, while all other structural parameters are kept identical to Unit-A.

2.4 Design of Basic Antenna Units

To confirm the finite array exhibits excellent radiation and scattering characteristics, an analysis of the performance of Unit-A and Unit-B is conducted. Figure 8 shows the active VSWRs of the two elements in the broadside and

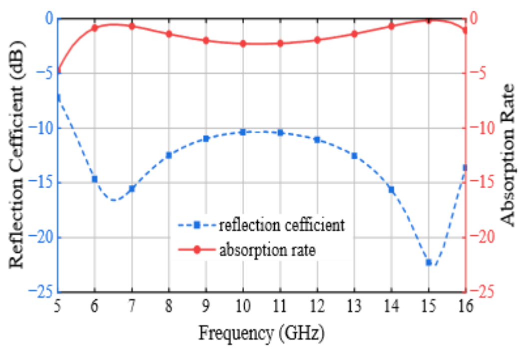

Fig. 6. Reflection coefficient and absorption rate of Unit-A under vertically incident cross-polarized waves.

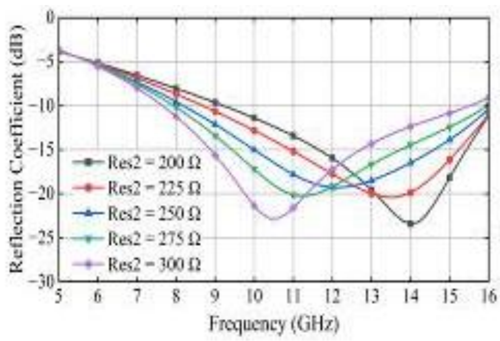

Fig. 7. Reflection coefficient of Unit-B loaded with different resistors under cross-polarized wave incidence.

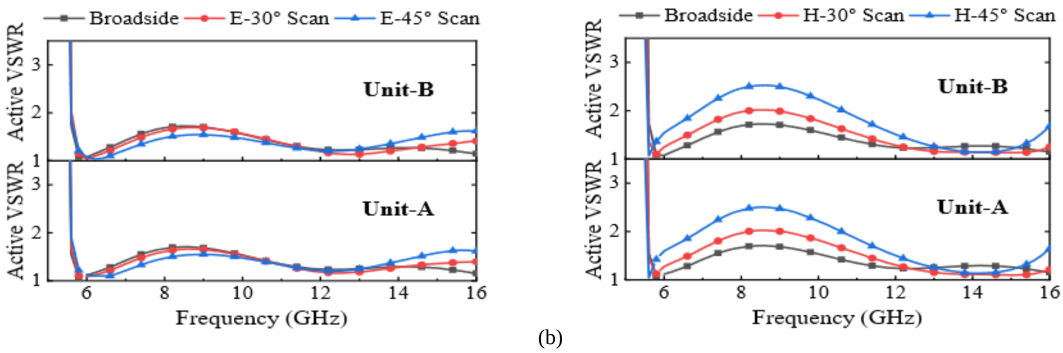

(a) (b)

Fig. 8. Active VSWR for different scanning angles of the low-scattering tightly coupled antenna: (a) E-plane; (b) H-plane.

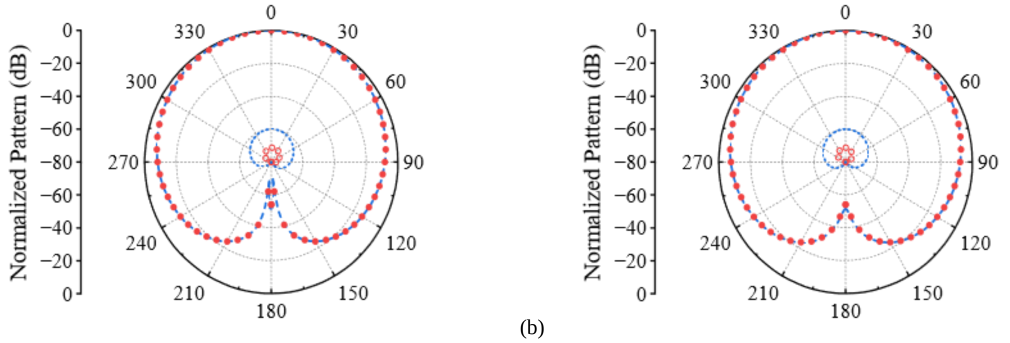

(a) (b)

Fig. 9. Simulated normalized radiation patterns of the proposed low-scattering element at 11 GHz: (a) E-plane; (b) H-plane.

and E-/H-plane. It can be observed that the active VSWRs of both antenna units are less than 2.0 from 5.6 to 16 GHz for broadside and 45° scanning in the E-plane. Compared to the simulation results of the reference antenna shown in Fig. 4(a), it is evident that adding a resistive metal strip improves the impedance matching characteristics at 45° E-plane in the high-frequency range. When scanning at 45° in the H-plane, the active VSWRs of both low-scattering broadband tightly coupled units remain below 2.6 within the operating frequency range, and the trend of the curves is consistent with that of the reference antenna.

The simulated E-plane and H-plane normalized radiation patterns at 11 GHz of both Unit-A and Unit-B are shown in Fig. 9(a) and (b). In these figures, the main polarization gain curves of Unit-A and Unit-B exhibit high overlap in both the E-plane and H-plane, with cross-polarization electrical gain consistently below −50 dB, which demonstrates excellent cross-polarization characteristics. Therefore, using a hybrid array configuration consisting of Unit-A and Unit-B does not negatively impact the array's radiation performance.

The scattering characteristics of the two antenna units under cross-polarized wave irradiation in an infinite-period environment are shown in Fig. 10, along with a comparison to the reference antenna element. As can be seen, the proposed low-scattering antenna Unit-A and Unit-B show a significant in-band (5–16 GHz) RCS reduction as compared with the reference antenna. In detail, Unit-A exhibits a monostatic RCS reduction of more than 10 dB over the 5.6–16 GHz range, while Unit-B shows a reduction greater than 15 dB within the 10–14.6 GHz range. Consequently, the hybrid array configuration of the two units can achieve complementary scattering reduction values within the corresponding frequency bands, thereby achieving a low-scattering design within a broad bandwidth.

3. Finite Array Simulation and Prototype Measurement

3.1 Low-Scattering Phased Array Structure

To validate the radiation and scattering characteristics of the designed triangular grid phased antenna array, a 10 × 10 low-scattering broadband phased array antenna is fabricated and assembled, as illustrated in Fig. 11. To achieve a maximally symmetrical distribution of the resistive

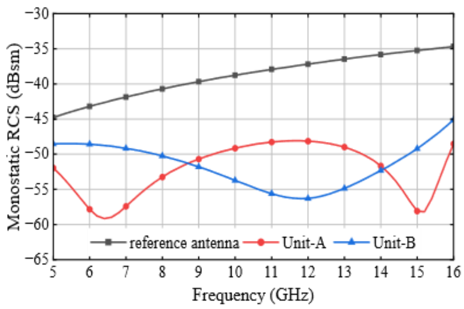

Fig. 10. Comparison of the monostatic RCS between the low-scattering units and the reference antenna element.

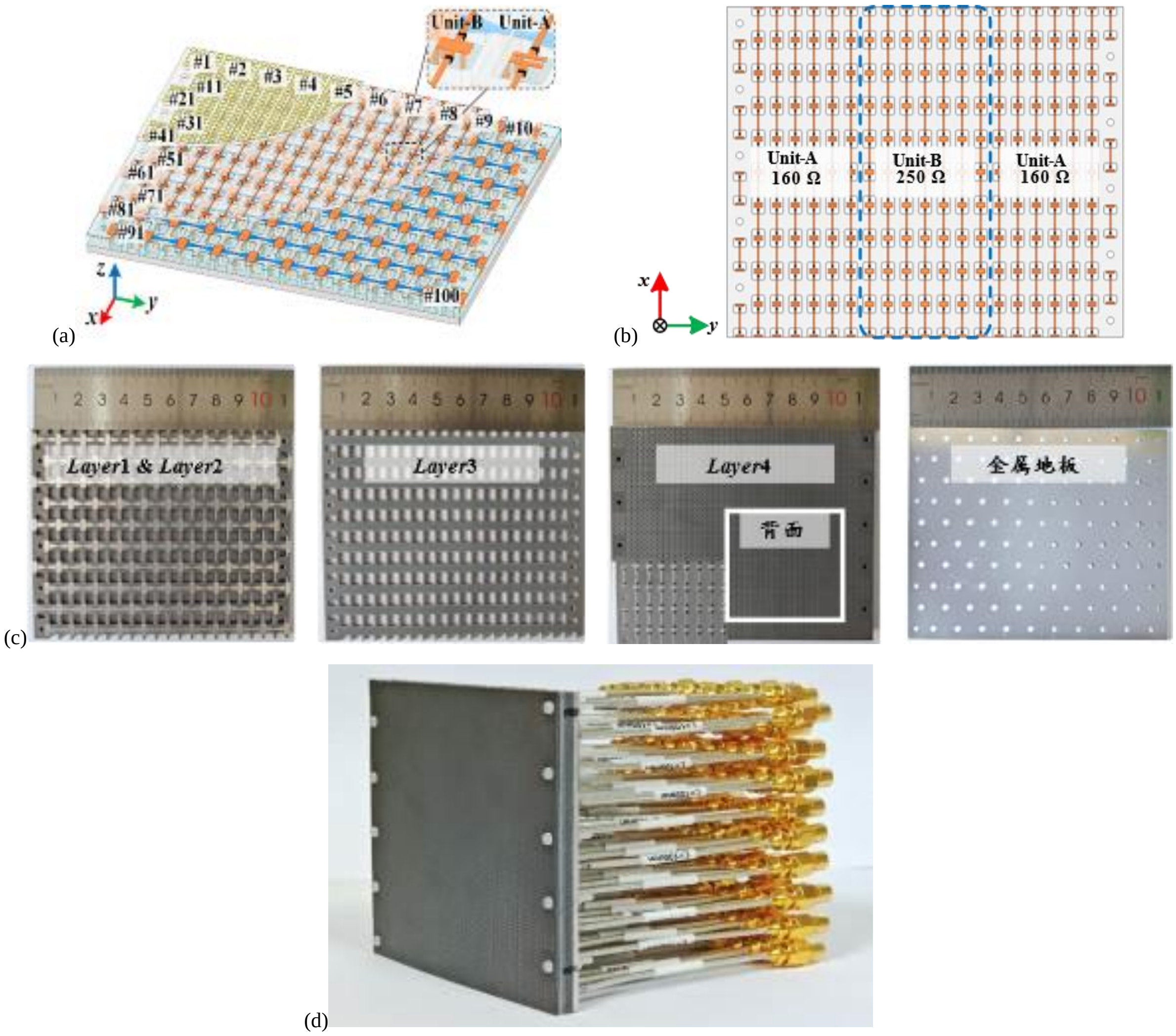

Fig. 11. Simulation model and principle prototype of 10 × 10 broadband low-scattering antenna array: (a) Finite array simulation model; (b) Resistive metallic strips; (c) Detailed diagram of the prototype; (d) Prototype.

metal strips within the triangular grid array while preserving the low-scattering characteristics, the strips are arranged as shown in Fig. 11(b). This configuration uses a total of 240 resistors of 160 Ω and 160 resistors of 250 Ω, all of which are surface-mount components with 0402 packaging (1 mm × 0.5 mm). Considering the truncation effects of the finite array, the outermost elements of the array are set as dummy elements, terminated with 50 Ω matched loads, with the actual excitation aperture being 8 × 8.

Furthermore, to evaluate the radiation scattering characteristics of the designed array, a 10 × 10 phased array antenna composed of reference antenna elements is selected as the reference array for comparison.

The low-scattering prototype is illustrated in Fig. 11(c) and (d). The dipole layer, coupled patch, and WAIM layers are all printed onto F4BM-2 substrate with a relative permittivity of 2.2, integrated onto a 2 mm-thick tin-plated brass reflector plate, which provides mechanical support for the antenna. Layer1 and Layer2 are laminated together into a single unit via PP lamination. Resistors are mounted on the bottom surface of Layer4, while the dielectric vias on Layer3 reserve space for surface-mount resistors. The inner conductor of the 50 Ω semi-flexible RF cable is connected to one end of the dipole arm, while the outer conductor is attached to the metal ground plane. Finally, the multi-layer dielectric substrate is fixed to the metal ground plane using nylon screws.

3.2 Radiation Performance of the Finite Array

The far-field radiation characteristic measuring environment is shown in Fig. 12. The scanning radiation pat-

Fig. 12. Prototype far-field radiation characteristics measuring environment.

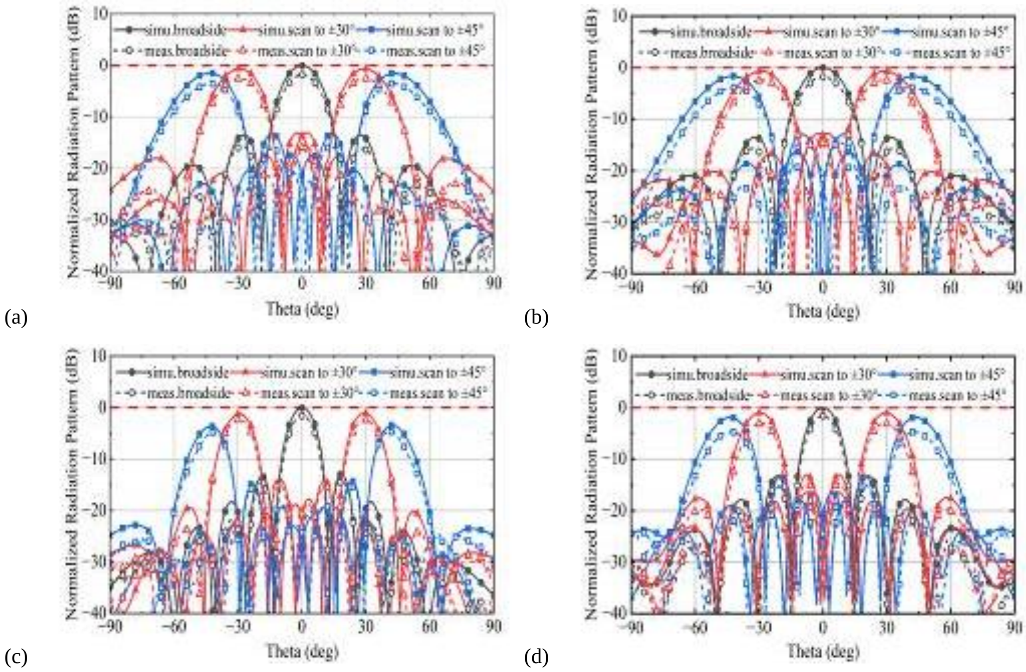

Fig. 13. Simulated and measured normalized radiation patterns of the low-scattering phased array antenna with triangular grid arrangement: (a) E-plane at 11 GHz; (b) H-plane at 11 GHz; (c) E-plane at 16 GHz; (d) H-plane at 16 GHz.

tern of the phased array antenna is measured using the unit excitation active element pattern (UEAEP) method [18]. The radiation pattern of the prototype is measured at the representative frequency of 11 GHz. Figure 13 presents the simulated and measured normalized radiation patterns of the low-scattering tightly coupled phased array antenna with a triangular lattice grid. The measured and simulated results demonstrate excellent agreement in the overall trends. The measurement error primarily arises from phase distortions introduced by repeated insertion and removal of the matched load and cables during the UEAEP measurements.

Figure 14 illustrates the variation of the broadside gain of the designed array with frequency, along with the simulated results of the reference array for comparison. It is evident that the co-polarization gain curves of the designed and reference arrays are basically similar, confirming that the proposed design approach does not cause a significant degradation in broadside gain. The measured gain curve of the prototype closely matches the simulated results, exhibiting a maximum gain deviation of 2 dB across the operating frequency band. The designed array achieves a simulated cross-polarization electrical average of less than −30 dB, and the measured average remains below −15 dB, which verifies that the array maintains excellent polarization purity.

3.3 Scattering Performance of the Finite Array

The scattering characteristic measuring environment is illustrated in Fig. 15. A pair of horn antennas operating in 1–18 GHz with an extremely small bistatic angle are connected to the vector network analyzer (R&S ZNB40) as the transmitters and receivers. The antenna under test, terminated with a matched load, is mounted on a foam turntable and aligned with the transceiver system. The experiment sequentially measures the scattering results of the environment and the prototype under test, and saves the measured data. Monostatic RCS results under normal incident waves are measured limited by the measurement environment. Following post-processing by the measurement system, the monostatic RCS of the prototype under test can be obtained.

Figure 16 shows the measured and simulated monostatic RCS patterns of both the design antenna array and the reference array under vertical incidences of cross-polarized waves. Besides, the monostatic RCS for a metal plate (PEC) of equivalent dimension is provided, with an aperture size of 92 × 111.3 mm². As can be observed, the monostatic RCS of the reference array shows a great agreement with the PEC. Comparing with the reference array,

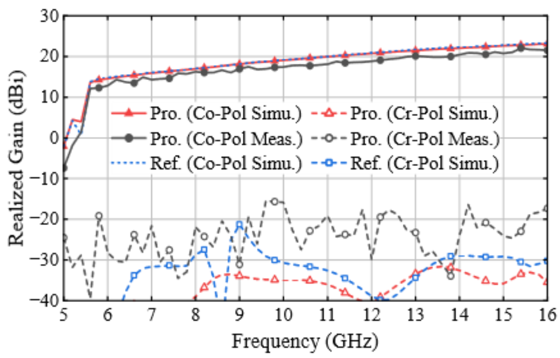

Fig. 14. Comparison between simulated and measured broadside radiation gain.

it can be seen that the designed array exhibits effective RCS reduction from 5 to 16 GHz, achieving a monostatic RCS reduction exceeding 10 dB in the 6.6–16 GHz band. Meanwhile, the RCS reduction band is consistent with the scattering characteristics of the tightly coupled antenna unit in Fig. 10, which verifies that the designed low-scattering array suppresses monostatic RCS under cross-polarized waves. Within the frequency band of 5 to 16 GHz, the simulated average RCS reduction amounted to 13 dB. Moreover, the measured results agree well with the simulated results, validating the reliability of the simulation method, while the observed discrepancies are primarily attributed to the resistance tolerance of the chip resistors.

To validate the bistatic RCS reduction effect of the designed low-scattering triangular grid phased array antenna, Figure 17 presents bistatic RCS of the designed array at 8 GHz and 14 GHz under cross-polarized wave vertical irradiation as compared with the reference array. As shown, the designed resistive strip does not cause an increase in dual-station scattering within other angular domains.

In practical applications, the low-scattering performance of antenna arrays under oblique incidence is considered equally important as that under normal incidence. Figures 18 and 19 show the simulated bistatic RCS reduction effect when cross-polarized waves are obliquely incident at different angles in the xoz-/yoz-planes, respectively. It is evident that the resistive metallic strips exhibit good absorption characteristics when illuminated by cross-polarized waves at oblique angles of 30°, 45°, and 60°, compared with the reference array. As the angle of incidence increases, the amount of reduction decreases accordingly. The peak scattering field under oblique incidence remains below −10 dBsm at the typical frequencies of 8 GHz and 14 GHz, which demonstrates excellent bistatic scattering characteristics. Consequently, the proposed antenna array effectively reduces RCS under oblique incident plane waves.

Fig. 15. Measurement environment of the prototype.

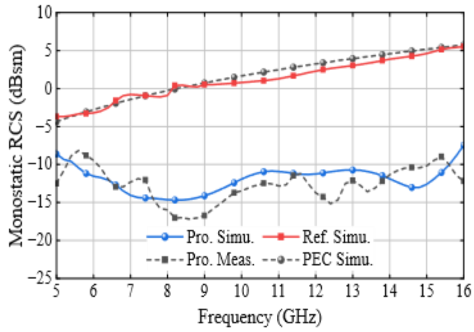

Fig. 16. Comparison of simulated and measured monostatic RCS.

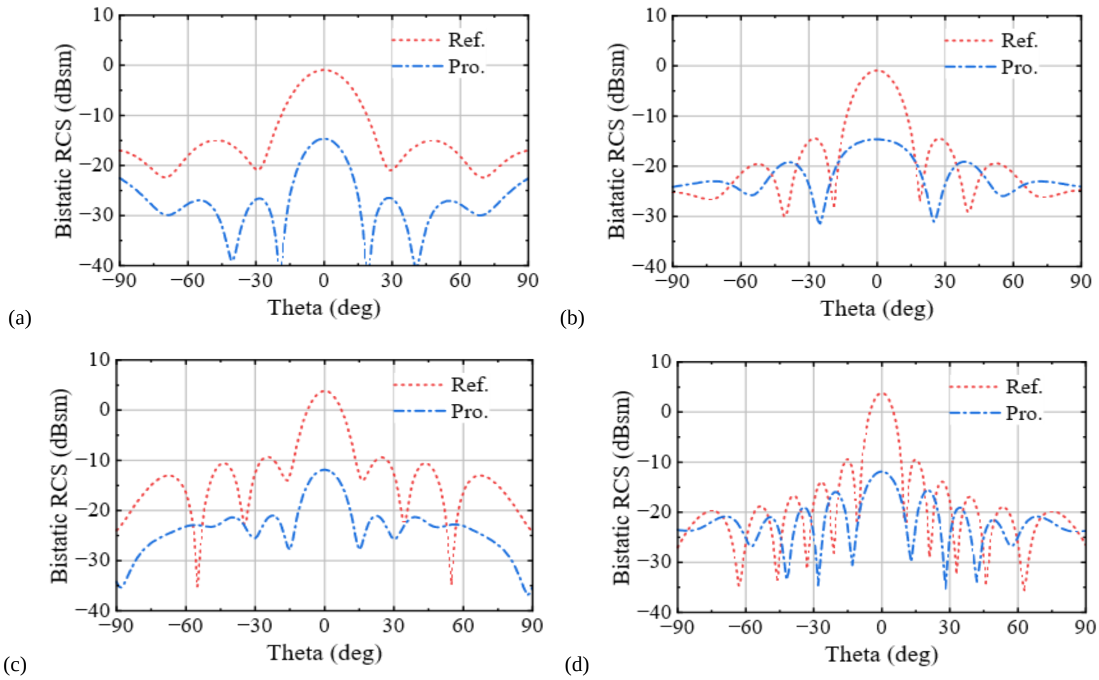

Fig. 17. Bistatic RCS simulated results for the proposed array and reference array under normal incidence for cross-polarized waves: (a) xoz plane at 8 GHz; (b) yoz plane at 8 GHz; (c) xoz plane at 14 GHz; (d) yoz plane at 14 GHz.

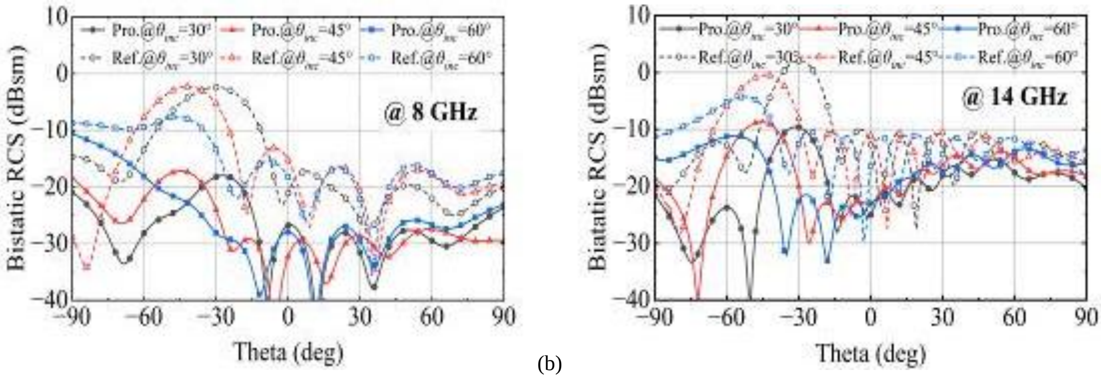

(a) (b)

Fig. 18. Bistatic RCS of the proposed and reference array under oblique incidence in xoz plane: (a) 8 GHz; (b).14 GHz.

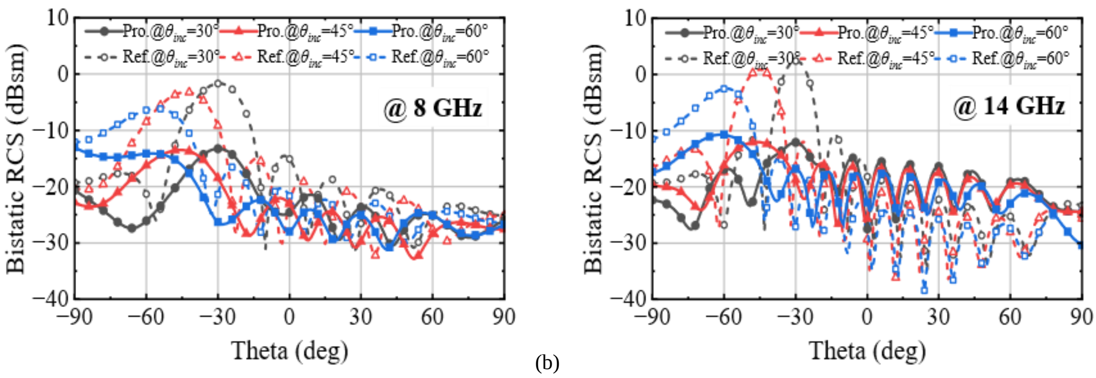

(a) (b)

Fig. 19. Bistatic RCS of the proposed and reference array under oblique incidence in yoz plane: (a) 8 GHz; (b) 14 GHz.

Refs.	Antenna Type	Radiation Performance	Scan Angle	Monostatic RCS Reduction (cross-polarized wave)	Grid Layout Array Pitch
[9]	Dipole array	7–21 GHz Active VSWR < 3	E-/H- ±45°	N.A.	Triangular grid 0.55 × 0.64 λ^2_{21GHz}
[11]	Microstrip patch array	14–21 GHz Active VSWR < 2	E-/H- ±50°	N.A.	Triangular grid 0.48 × 0.48 λ^2_{16GHz}
[19]	Microstrip patch array	9.8–11.1 GHz Active VSWR < 2	E- ±51° H- ±33°	N.A.	Triangular grid 1 × 1 λ^2_{11GHz}
[15]	Vivaldi array	8–12 GHz Active VSWR < 2	E-/H- ±60°	8–12 GHz RCSR > 0 dB	Triangular grid 0.48 × 0.52 λ^2_{12GHz}
[20]	Tightly coupled array	6–18 GHz Active VSWR < 3	E-/H- ±45°	8–12 GHz RCSR > 5 dB	Rectangular grid 0.36 × 0.36 λ^2_{18GHz}
This work	**Tightly coupled array**	**5.6–16 GHz Active VSWR < 2.6**	**E-/H- ±45°**	**6.6–16 GHz RCSR > 10 dB**	**Triangular grid 0.49 × 0.57** λ^2_{16GHz}

Tab. 2. Performance comparison with reported designs.

To further indicate the excellent merits of this work, the performances of the proposed low-scattering phased antenna array under a triangular grid are compared to other literature associated with phased arrays, as summarized in Tab. 2. Among the reported and proposed works, the proposed low-scattering phased array with a triangular lattice arrangement exhibits a favorable performance in terms of bandwidth, wide-angle scanning, and low-scattering. It achieves excellent radiation performance from 5.6 to 16 GHz, while enabling scanning up to ±45° in both E- and H-planes. More importantly, the triangular lattice grid allows compact element placement, which effectively suppresses array scattering and achieves a monostatic RCS reduction exceeding 10 dB across the band.

4. Conclusion

In this paper, a low-scattering phased array antenna based on a triangular grid arrangement with resistive metallic strips is proposed. A 10 × 10 triangular lattice phased array prototype is fabricated and measured to validate the design, and the simulated and measured results are in great agreement. Specifically, the proposed low-scattering array achieves an effective in-band RCS reduction under cross-polarized incidence, while maintaining good radiation performance. The proposed array provides an effective solution for achieving wideband radiation and low-scattering characteristics, which are promising for modern low-observable array antenna applications.

Acknowledgments

Funding: This work was supported in part by the National Natural Science Foundation of China under Grant 62301409, and Open Fund of National Key Laboratory of Electromagnetic Information Control and Effects under Grant SYS1W2024030413 and SYS1W2023010101.

References

[1] HOSSAIN, M. M., KOULOURIDIS, S., VENKATAKRISHNAN, S. B., et al. Simple wideband circularly polarized tightly coupled dipole array. *IEEE Antennas and Wireless Propagation Letters*, 2024, vol. 23, no. 6, p. 1929–1933. DOI: 10.1109/LAWP.2024.3374578

[2] WU, J., LI, Z., SUN, H. Design and performance of a fully-polarized tightly-coupled patch antenna for advanced phased array radar systems. *Progress In Electromagnetics Research Letters*, 2024, vol. 121, p. 41–49. DOI: 10.2528/PIERL24051302

[3] WANG, B., YANG, S., ZHANG, Z., et al. Ferrite-loaded ultralow profile ultrawideband tightly coupled dipole array. *IEEE Transactions on Antennas and Propagation*, 2022, vol. 70, no. 3, p. 1965–1975. DOI: 10.1109/TAP.2021.3118798

[4] GAO, G., DAI, J., LIU, S., et al. Low in-band-RCS tightly coupled dipole array based on metamaterial absorber. In *2024 International Applied Computational Electromagnetics Society Symposium (ACES-China)*. Xi'an (China), 2024, p. 1–3. DOI: 10.1109/ACES-China62474.2024.10699542

[5] SUN, J. X., CHENG, Y. J., WU, Y. F., et al. Ultrawideband, low-profile, and low-RCS conformal phased array with capacitance-integrated balun and multifunctional meta-surface. *IEEE Transactions on Antennas and Propagation*, 2022, vol. 70, no. 9, p. 7448–7457. DOI: 10.1109/TAP.2022.3183301

[6] ZHANG, Z., WANG, B., YANG, F., et al. Conical conformal tightly coupled dipole arrays co-designed with low-scattering characteristics. *IEEE Transactions on Antennas and Propagation*, 2022, vol. 70, no. 12, p. 12352–12357. DOI: 10.1109/TAP.2022.3209732

[7] FANG, S.-G., QU, S.-W. Broadband wide-scanning large-curvature cylindrical conformal dipole array antenna with low-scattering characteristics. *IEEE Transactions on Antennas and Propagation*, 2024, vol. 72, no. 8, p. 6437–6447. DOI: 10.1109/TAP.2024.3417293

[8] MAILLOUX, R. *Phased Array Antenna Handbook*. 3rd ed., Norwood (USA): Artech House, 2017. ISBN: 9781630815080

[9] MANIVANNAN, P., VOUVAKIS, M. N. Differentially-fed coincident phase-centered wideband dipole array on a triangular grid. In *2024 IEEE International Symposium on Antennas and Propagation and INC/USNC-URSI Radio Science Meeting (AP-S/INC-USNC-URSI)*. Firenze (Italy), 2024, p. 855–856. DOI: 10.1109/AP-S/INC-USNC-URSI52054.2024.10687077

[10] KINDT, R. W., BINDER, B. T. Wideband planar printed aperture on a triangular lattice for millimeter wave applications. In *2023 17th European Conference on Antennas and Propagation (EuCAP)*. Florence (Italy), 2023, p. 1–3. DOI: 10.23919/EuCAP57121.2023.10133722

[11] LI, X., SONG, X., YIN, J., et al. A triangular grid millimeter wave planar array with wide bandwidth and angular scanning. In *2024 Cross Strait Radio Science and Wireless Technology Conference (CSRSWTC)*.Macao (China), 2024, p. 1–3. DOI: 10.1109/CSRSWTC64338.2024.10811645

[12] VISHWAKARMA, M., NAGARAJA RAO, P. Performance investigation of triangular lattice arrangement based UWB phased array for electronic warfare applications. In *2024 IEEE Microwaves, Antennas, and Propagation Conference (MAPCON)*. Hyderabad (India), 2024, p. 1–6. DOI: 10.1109/MAPCON61407.2024.10923352

[13] KINDT, R. W., BINDER, B. T. Wideband, low-profile, dual-polarized machined-metal array on a triangular lattice. *IEEE Transactions on Antennas and Propagation*, Feb. 2022, vol. 70, no. 2, p. 1097–1106. DOI: 10.1109/TAP.2021.3111317

[14] TAO, J., LI, X., TENG, F., et al. ±45° dual-slant polarized all-metal Vivaldi array with isosceles triangular lattice. *Electromagnetics*, 2026 vol. 46, no. 4, p. 507–523. DOI: 10.1080/02726343.2025.2566765

[15] ZHANG, T., CHEN, Y., LIU, Z., et al. A low-scattering Vivaldi antenna array with slits on nonradiating edges. *IEEE Transactions on Antennas and Propagation*, 2023, vol. 71, no. 2, p. 1999–2004. DOI: 10.1109/TAP.2022.3232690

[16] SHARP, E. A triangular arrangement of planar-array elements that reduces the number needed. *IEEE Transactions on Antennas and Propagation*, 1961, vol. 9, no. 2, p. 126–129. DOI: 10.1109/TAP.1961.1144967

[17] WANG, B., YANG, S., CHEN, Y., et al. Low cross-polarization ultrawideband tightly coupled balanced antipodal dipole array. *IEEE Transactions on Antennas and Propagation*, 2020, vol. 68, no. 6, p. 4479–4488. DOI: 10.1109/TAP.2020.2970087

[18] POZAR, D. M. The active element pattern. *IEEE Transactions on Antennas and Propagation*, 1994, vol. 42, no. 8, p. 1176–1178. DOI: 10.1109/8.310010

[19] PAN, Y., HUANG, Z., LIAO, S. Large phase-shifting channel spacing phased array antenna with triangular grid. In *2025 18th IEEE United Conference on Millimeter Waves and Terahertz Technologies (UCMMT)*. Nanjing (China), 2025, p. 1–3. DOI: 10.1109/UCMMT67044.2025.11286411

[20] GOU, Y., CHEN, Y., YANG, S. A tightly coupled dipole array with diverse element reflection phases for RCS reduction. *Chinese Journal of Electronics*, 2024, vol. 33, no. 2, p. 449–455. DOI: 10.23919/cje.2022.00.121